引用格式：LIANG Tiantian, HONG Yinghao, MA Yufei. Cylindrical Cavity-based Quartz-enhanced Spectroscopy Sensing (Invited)[J]. Acta Photonica Sinica, 2023, 52(3):0352113
梁添添,洪颖昊,马欲飞.基于圆柱腔的石英增强光谱传感技术研究(特邀)[J].光子学报,2023,52(3):0352113

基于圆柱腔的石英增强光谱传感技术研究（特邀）

梁添添,洪颖昊,马欲飞
(哈尔滨工业大学 航天学院 可调谐激光技术国家级重点实验室,哈尔滨 150001)

摘　要:设计了一种非一维共振腔的圆柱腔,利用入射声波与反射声波之间的共振增强效应来增大传感系统信号强度,并应用在面外入射的石英增强光声光谱技术(QEPAS)和石英增强光致热弹光谱技术(LITES)技术中。对添加圆柱腔前后的石英音叉摆幅和圆柱腔位置进行了理论模拟与优化。实验中,采用水汽为目标探测气体和输出波长1.395 μm的半导体激光器为激发源,相比未添加圆柱腔的裸石英音叉系统,添加圆柱腔的QEPAS和LITES系统探测极限分别改善了2.32倍和1.27倍。

关键词:石英增强光声光谱技术;石英增强光致热弹光谱技术;圆柱腔;气体传感;石英音叉
中图分类号:O433.4　　**文献标识码**:A　　**doi**:10.3788/gzxb20235203.0352113

0　引言

近年来,大气环境污染、碳中和与碳达峰等环境问题、以及各种危险气体引起的爆炸等问题日益引起人们的关注[1-2]。气体传感技术气可对气体的浓度进行高灵敏地检测,在上述场合中有着重要的应用。气体传感技术可分为非光谱式与光谱式,相比非光谱式,光谱式气体传感利用了气体分子的特征指纹谱,因此具有优异的选择性,同时其还具有在线测量、非侵入式、灵敏度高等优点,是目前气体传感领域研究的热点[3-5]。

光声光谱利用光声效应产生声波信号,采用麦克风对其进行探测,进而反演出气体浓度,是一种零背景光谱技术[6-7],因而在气体传感领域应用广泛。但麦克风响应频带较宽,因而容易受环境噪声的影响,此外,麦克风光声光谱系统含有光声池,因而体积较大[8],这些均对其实际应用产生了不利影响。为了克服上述缺点,2002年,美国莱斯大学TITTEL F教授课题组提出了石英增强光声光谱技术(Quartz-enhanced Photoacoustic Spectroscopy, QEPAS)[9],该技术采用石英音叉(Quartz Tuning Fork, QTF)对声波信号进行探测,其较窄的响应频带(~4 Hz)、高Q值(~10 000)、以及不需要光声池,使得它具有抗噪声、体积小等优点[10-11],且为了进一步提高其信号强度,多种微型化的一维声波微共振腔被添加在石英音叉的两端,形成声波驻波场,常见的微共振腔有on-beam型、off-beam型、T型、H型等[12-15]。尽管QEPAS技术应用广泛,但由于其工作原理的限制,石英音叉需要与待测气体进行接触,因此QEPAS技术是一种接触式的测量技术,这就限制了它在氧化性、腐蚀性气体测量中的应用[16-17]。为了解决这个问题,2018年,哈尔滨工业大学科研团队提出了石英增强光致热弹光谱技术(Light-induced Thermoelastic Spectroscopy, LITES)[18],LITES技术利用石英音叉的光致热弹效应[19-20],将待测气体与石英音叉进行分离,因而很好地解决了这个问题。基于QEPAS和LITES技术的优点,这两种技术目前发展迅速,被广泛应用在各种各样痕量气体的检测应用中。

气体传感技术研究一个重要方向就是进一步改善其检测极限,以满足更多领域的应用要求。基于此,本文将圆柱腔引入到石英增强光谱技术中,这种圆柱腔与以前广泛报道的一维声波微共振腔不同,利用的

基金项目:国家自然科学基金(Nos. 62022032,61875047,61505041),黑龙江省优秀青年科学基金(No. YQ2019F006),黑龙江省博士后科研启动金(No. LBH-Q18052),中央高校基本科研业务费专项资金
第一作者:梁添添, 21s021041@stu.hit.edu.cn
通讯作者:马欲飞, mayufei@hit.edu.cn
收稿日期:2022-05-20;**录用日期**:2022-06-15

是入射声波与反射声波之间的共振增强效应。在本文中，首先对圆柱腔增强效果进行理论模拟，计算了石英音叉在各种不同条件下的摆幅，随后开展了基于圆柱腔的QEPAS和LITES相关实验，以验证其增强效果。

1 圆柱腔增强原理

QEPAS和LITES技术的原理分别如图1(a)和1(b)所示。在QEPAS技术中，基于光声效应的原理，受波长调制的入射激光能量被气体分子吸收后将产生一定频率的声波，石英音叉作为压电材料，受该声波扰动后将产生压电信号，该信号的强度与气体浓度相关，故而可用于气体浓度的反演[21]。而在LITES技术中，受波长调制的激光束将穿过待测气体，同时能量被气体吸收，最后入射在石英音叉上，由于石英音叉具有热弹效应，吸收强度周期性变化的激光能量后，将产生热弹形变，进而产生机械摆动，摆动的石英音叉可视为产生声波的声源[22]。

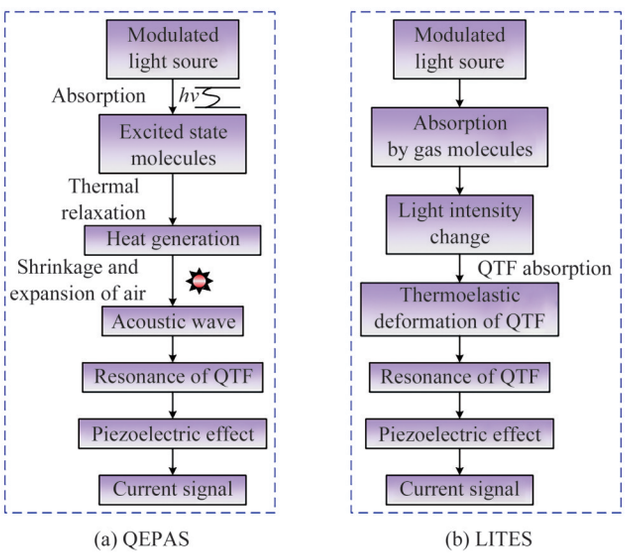

图1 QEPAS和LITES技术原理

Fig. 1 Principle of QEPAS and LITES

入射声波从空气中传播到圆柱腔时，由于介质的改变，声波会在腔的内壁界面发生反射，当圆柱腔折射率高于空气时，将在反射时产生半波损失进而导致声波的传播方向和相位发生改变。在基于圆柱腔增强的QEPAS/LITES技术中，入射声波和反射声波叠加形成驻波后将增强声波信号，进而提高系统的灵敏度，而驻波的形成需满足两列波的振幅相同的条件，因此要增强圆柱腔内的声波信号，入射声波和反射声波的振幅不能相差太大。反射声波的能量与圆柱腔的材料有关，圆柱腔的内壁越光滑，反射的能量损失越小，反射声波的振幅也越接近入射声波。因此，本研究选用的是内壁光滑的不锈钢圆柱腔。

1.1 裸石英音叉QEPAS系统仿真

首先在COMSOL软件中根据共振频率为32.768 kHz的标准石英音叉的尺寸参数建立相应的物理模型，将石英音叉的材料属性设置为Quartz LH (1 949 IRE)，并定义石英音叉为压电材料。为更真实地模拟其振动，对其底部边界进行了固定约束，仿真得到的石英音叉频率为32.747 kHz。考虑到声波在空气中传输时将保持传输方向不变并不断衰减直至消失。为充分模拟实际情况，本文在石英音叉的外围添加了一个厚度一定、内径为r的球体，并将其作为完美匹配层以吸收多余的声波，除石英音叉外的整个球体被设为空气域，并将其内空气压强设为标准气压。而后，引入线源并将其类型设置为流动，以模拟光声效应产生的声波在空气中的传播。最后在声-结构边界中，选中石英音叉的全部边界，研究石英音叉的表面声压、摆幅等特性。

在QEPAS技术中，为使石英音叉摆幅最大，线源被设在距离石英音叉顶部0.7 mm的位置[23]。在石英音叉的共振频率下对裸石英音叉模型进行仿真研究，结果如图2所示。石英音叉表面的最大声压为4.42 mPa，最大摆幅为2.76×10^{-7} mm。从图2可知，声压作用在叉指内表面，并使石英音叉产生对称振动。

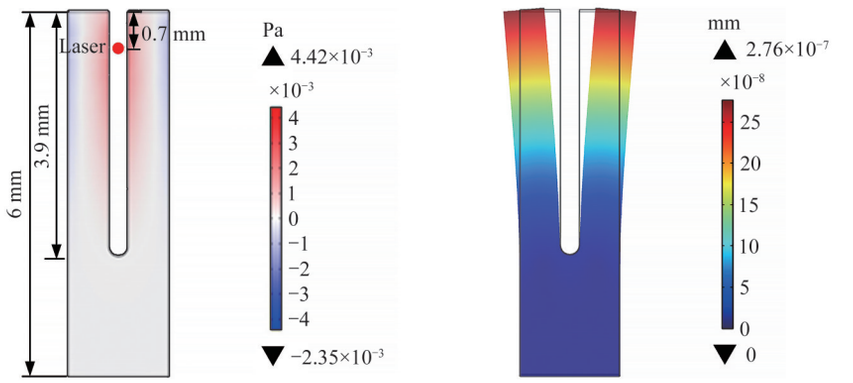

(a) The surface sound pressure for the bare QTF　　(b) The amplitude of swing for the bare QTF

图2　QEPAS系统中的裸石英音叉仿真结果

Fig. 2　Simulation results for the bare QTF in the QEPAS system

1.2　裸石英音叉LITES系统仿真

相较于QEPAS技术而言，LITES技术中激光并非穿过石英音叉叉指间隙，而是直接照射在石英音叉上。在LITES模型仿真中，线源的位置设置在石英音叉的根部，以实现最强的信号强度[24]。另外，为了减小模型的计算量，线源的长度设置为5 mm。LITES技术的原理是光致热弹性效应，石英音叉吸收激光能量后膨胀产生热应力，因此主要研究该模型的物理场为固体力学，故仅通过固体力学中石英音叉的摆幅便可反映其性能。仿真得到的基于LITES技术的石英音叉摆幅如图3所示，其最大摆幅为1.52×10^{-7} mm。

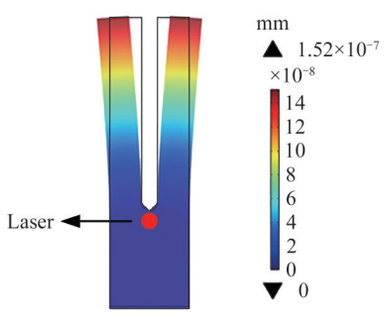

图3　LITES系统中的裸石英音叉摆幅

Fig. 3　The amplitude of swing for the bare QTF in the LITES system

1.3　基于圆柱腔的QEPAS系统仿真

在1.1节裸石英音叉仿真的基础上，本节研究了圆柱腔对QEPAS系统的影响，石英音叉与圆柱腔的物理模型如图4所示。

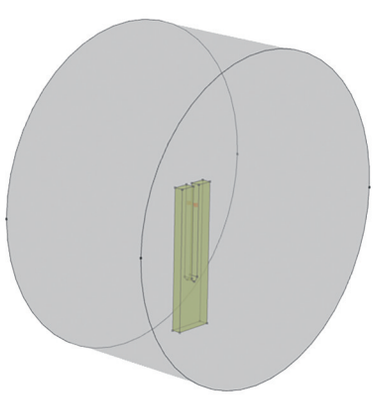

图4　基于圆柱腔的QEPAS仿真模型

Fig. 4　The simulation mode of cylindrical cavity-based QEPAS system

根据面内入射的研究结果[25]，当圆柱腔的半径设定为6.4 mm时可实现较为理想的驻波场。因此本文将圆柱腔的半径设定为6.4 mm，激光束位于圆柱腔中心，石英音叉与激光束之间的位置关系与1.1节中相同。添加圆柱腔后石英音叉表面的最大声压以及石英音叉摆幅仿真结果如图5所示，石英音叉的最大表面声压为16.46 mPa，最大摆幅为1.02×10^{-6} mm。对比1.1节中裸石英音叉系统的表面声压4.42 mPa和摆幅2.76×10^{-7} mm，圆柱腔对石英音叉的最大表面声压和摆幅有3.7倍的增强效果。

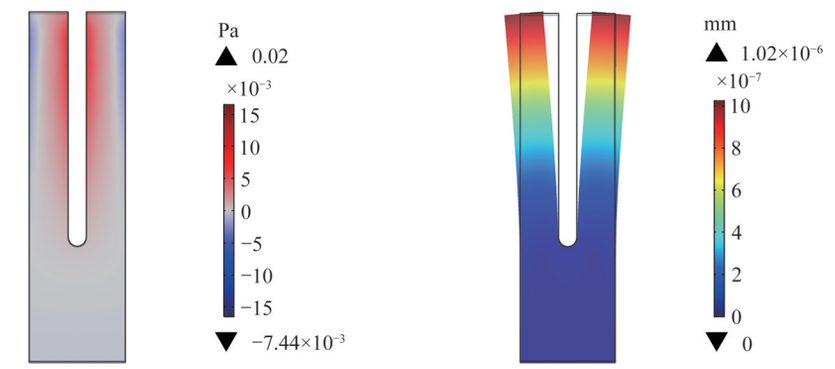

(a) The surface sound pressure for the QTF　　(b) The amplitude of swing for the QTF

图5 基于圆柱腔的QEPAS系统石英音叉仿真结果

Fig. 5 Simulation results for the QTF in cylindrical cavity-based QEPAS system

1.4 基于圆柱腔的LITES系统仿真

在裸石英音叉LITES系统的基础上，在石英音叉外部添加半径为6.4 mm的圆柱腔。为研究圆柱腔中心位置对石英音叉摆幅的影响，分别将圆柱腔中心设置在线源位置处和距离石英音叉顶部0.7 mm位置处（即声波作用石英音叉的最佳高度处）。仿真的结果如图6所示，两种情况下石英音叉的摆幅分别为1.73×10^{-7} mm和2.87×10^{-7} mm，即当圆柱腔中心在距离石英音叉顶部0.7 mm时对石英音叉的摆幅增强效果较好，相比1.2节中的裸石英音叉系统有1.9倍的改善。LITES技术产生声波的声源可视为在距离石英音叉顶部0.7 mm的位置处，因此当圆柱腔中心在距离石英音叉顶部0.7 mm处时声波的耦合效果最好。而当圆柱腔中心在激光位置处（叉指根部位置），经圆柱腔耦合的声波强度较弱。因此，在后续的实验中，圆柱腔中心将被设置在距离石英音叉顶部0.7 mm位置处。

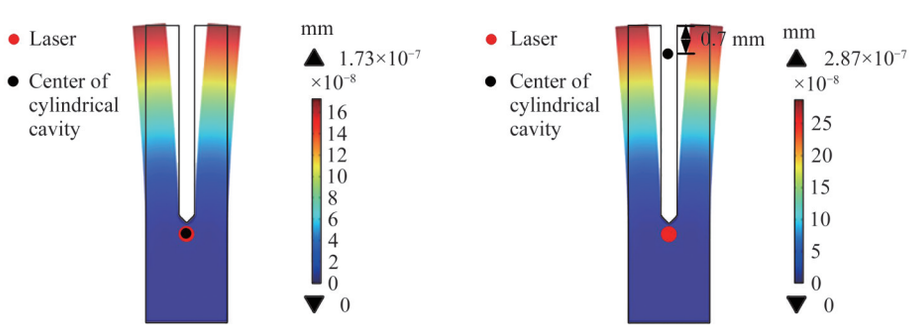

(a) The center of the cylindrical cavity located at the laser position (the root of the QTF)　　(b) The center of the cylindrical cavity located at 0.7 mm below the top of the QTF

图6 基于圆柱腔的LITES系统石英音叉仿真结果

Fig. 6 Simulation results for the QTF in cylindrical cavity-based LITES system

2 实验装置

基于圆柱腔QEPAS/LITES痕量气体探测系统如图7所示，实验中选用共振频率为32.768 kHz的石英音叉（真空下）。本文选用水汽作为目标气体，并选择位于7 168.43 cm^{-1}处水汽谱线作为吸收线，该处吸收线的线强为1.196×10^{-20} cm/molecule，并可以免受空气中其他气体分子的干扰[26]。本文所用激光源的中心波长为1.395 μm以匹配水汽吸收线，其在水汽吸收峰处的输出功率为18.9 mW。为了充分利用光声效应所

产生的声波，圆柱腔采用反射率较大的304不锈钢材料进行加工，并在圆柱腔的侧面加工一个稍大于石英音叉尺寸的小孔使音叉能够放入腔内。信号发生器用来控制激光器电流使其扫描覆盖所选的水汽吸收线。锁相放大器输出的正弦波用于调制激光器波长，同时其还被用于光谱信号的解调，以得到二次谐波信号。锁相放大器的滚动系数设置为18 dB/oct，另外在进行二次谐波测量时，锁相放大器的积分时间被设置为100 ms。QEPAS、LITES痕量气体探测系统分别如图7（a）和（b）所示。

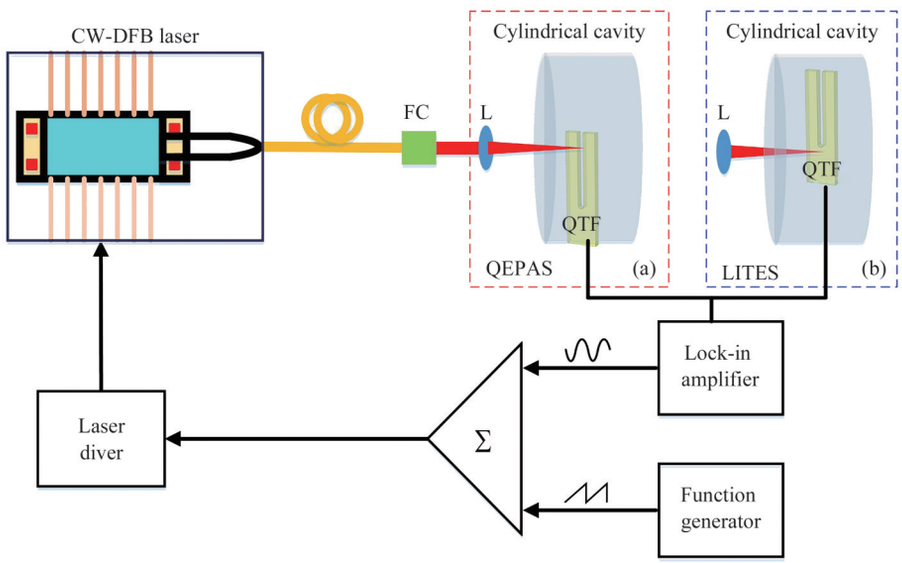

图7　基于圆柱腔的QEPAS/LITES系统结构示意图

Fig. 7　Schematic diagram of the cylindrical cavity-based QEPAS/LITES sensor systems

3　结果讨论与分析

3.1　基于圆柱腔增强的QEPAS传感

首先对裸石英音叉系统的特性进行了测量。裸石英音叉的频率响应如图8所示，通过洛伦兹函数拟合得到石英音叉的共振频率f_0=32 767.16 Hz、Q=13 611。添加圆柱腔后，系统的f_0降至32 766.88 Hz，Q值降为11 943，可见圆柱腔对系统的声波能量有一定的耦合作用。

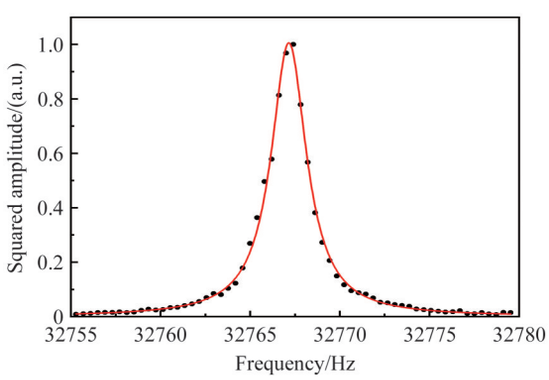

图8　裸石英音叉系统的频率响应曲线

Fig. 8　Response curve for bare QTF

为了使系统获得最强的响应，激光波长调制深度需要优化。调制深度的测量结果如图9所示，可见，系统的最佳调制深度为0.43 cm^{-1}。

在最佳共振状态和最佳调制深度下，分别测量了基于裸石英音叉和圆柱腔增强的QEPAS系统的2f信号，如图10所示。未添加圆柱腔时，系统的2f信号幅值为4.82 μV。添加圆柱腔后，系统的2f信号幅值为10.68 μV，增加了2.22倍。

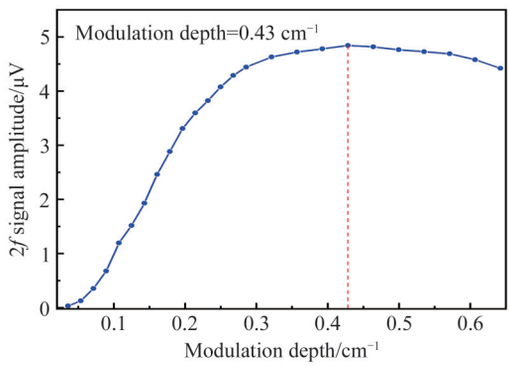

图 9 裸石英音叉系统的 $2f$ 信号幅值随调制深度的变化曲线

Fig. 9 The relationship between $2f$ signal amplitude of bare QTF based QEPAS system and laser modulation depth

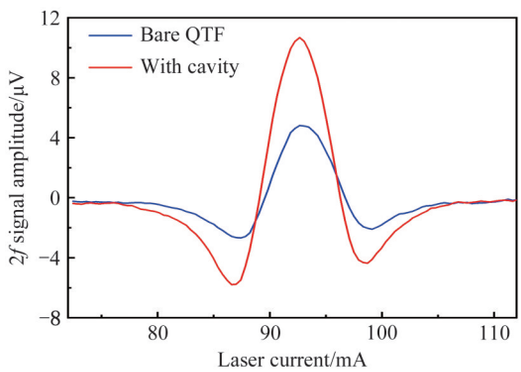

图 10 添加圆柱腔前后的 QEPAS 系统 $2f$ 信号

Fig. 10 $2f$ signal for QEAS sensor with and without cylindrical cavity

系统噪声如图 11 所示，对比可以看出添加圆柱腔后系统的噪声基本上不变。根据 $2f$ 信号、噪声以及环境的水汽浓度 0.57%，分别计算相应的信噪比（Signal to Noise Ratio，SNR）和最小探测极限（Minimum Detection Limit，MDL），如表 1 所示，添加圆柱腔后系统的最小探测极限改善了 2.32 倍。圆柱腔 QEPAS 系统的性能提升效果与 1.3 节中仿真结果有所偏差，这是因为仿真中网格的分割程度、音叉的压电转换效率均与实际有所偏差；另外在仿真得到的石英音叉的共振频率为 32.747 kHz，仿真得到的最佳参数下的圆柱腔能与该频率音叉能产生最佳耦合，而实际所用的标准石英音叉其共振频率测量值为 32.767 kHz，此频率的音叉与仿真得到最佳参数下的圆柱腔并非最佳耦合。这些原因都导致了实际的实验结果与仿真结果有所偏差。

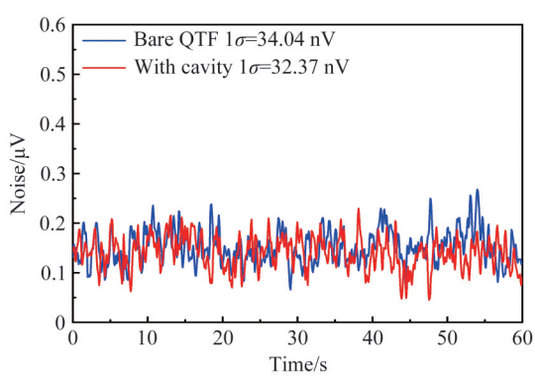

图 11 添加圆柱腔前后的 QEPAS 系统噪声

Fig. 11 Noise for QEAS sensor with and without cylindrical cavity

表1　添加圆柱腔前后的QEPAS系统性能

Table 1　Performance for QEAS sensor with and without cylindrical cavity

	2*f* signal/μV	Noise/nV	SNR	MDL/ppm
Bare QTF	4.82	34.04	142	40.14
With cylindrical cavity	10.68	32.37	330	17.27

3.2　基于圆柱腔增强的LITES传感

与3.1节类似，在最佳共振状态和最佳调制深度下，分别测量了基于裸石英音叉和圆柱腔的LITES系统的2*f*信号，如图12所示。未添加圆柱腔时，系统的2*f*信号幅值为40.29 μV，添加圆柱腔后，系统的2*f*信号幅值为49.61 μV，增加了1.23倍。

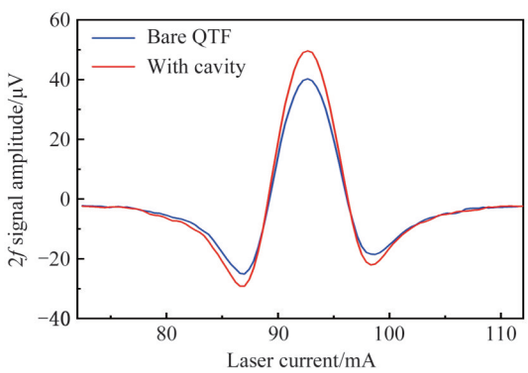

图12　添加圆柱腔前后的LITES系统2*f*信号

Fig.12　2*f* signal for LITES sensor with and without cylindrical cavity

系统噪声如图13所示，可以看出添加圆柱腔后系统的噪声幅值基本上未发生变化，但相比QEPAS系统，LITES系统的噪声幅值较高，这主要是因为在LITES技术中，激光束入射在石英音叉的根部，石英音叉吸收了部分激光能量，导致其热噪声变大。

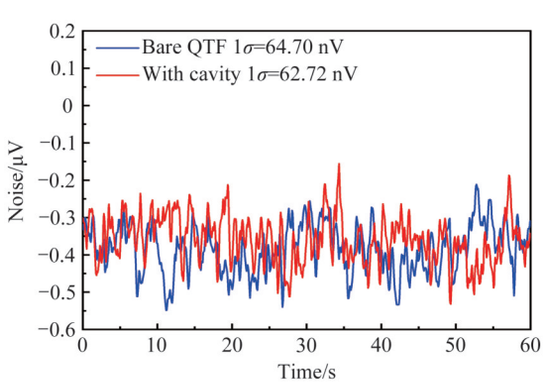

图13　添加圆柱腔前后的LITES系统噪声

Fig.13　Noise for LITES sensor with and without cylindrical cavity

根据2*f*信号、噪声幅值以及环境的水汽浓度0.57%，分别计算出相应的信噪比和最小探测极限，如表2所示。可见，添加圆柱腔前后的最小检测极限分别是9.15 ppm（1 ppm=1×10^{-6}）和7.21 ppm，添加圆柱腔系统性能改善了1.27倍。圆柱腔LITES系统的实验结果与仿真结果有所偏差的原因与3.1节中的QEPAS系统类似。

表2　添加圆柱腔前后的LITES系统性能

Table 2　Performance for LITES sensor with and without cylindrical cavity

	2*f* signal/μV	Noise/nV	SNR	MDL/ppm
Bare QTF	40.29	64.70	623	9.15
With cylindrical cavity	49.61	62.72	791	7.21

4 结论

基于石英音叉探测的QEPAS和LITES技术具有体积小、价格便宜、灵敏度高等优点，近年来发展迅速。在常见的QEPAS技术中，一般均采用一维微共振腔来增大信号强度。本文设计了一种圆柱腔，利用入射声波与反射声波之间的共振增强效应来增大传感系统信号强度，并应用在面外入射的QEPAS和LITES技术中。论文对添加圆柱腔前后的石英音叉摆幅和圆柱腔位置进行了理论模拟与优化，验证了设计的正确性。在实验研究中，相比未添加圆柱腔的裸石英音叉系统，添加圆柱腔的QEPAS系统探测极限改善了2.32倍，添加圆柱腔的LITES系统探测极限改善了1.27倍。研究结果标明，圆柱腔是一种改善探测能力的通用有效手段，可提升QEPAS和LITES技术的性能。

参考文献

[1] KOCACHE R. The measurement of oxygen in gas-mixtures[J]. Journal of Physics E: Scientific Instruments, 1986, 19(6): 401-412.

[2] KHALIL M A K, RASMUSSEN R A. Carbon monoxide in the earth's atmosphere: increasing trend[J]. Science, 1984, 224(4644): 54-56.

[3] WOJTAS J, TITTEL F K, STACEWICZ T, et al. Cavity-enhanced absorption spectroscopy and photoacoustic spectroscopy for human breath analysis[J]. International Journal of Thermophysics, 2014, 35(12): 2215-2225.

[4] MILDE T, HOPPE M, TATENGUEM H, et al. QEPAS sensor for breath analysis: a behavior of pressure[J]. Applied Optics, 2018, 57(10): C120-C127.

[5] MA Y F, LEWICKI R, RAZEGHI M, et al. QEPAS based ppb-level detection of CO and N_2O using a high power CW DFB-QCL[J]. Optics Express, 2013, 21(1): 1008-1019.

[6] ELIA A, LUGARA P M, DI FRANCO C, et al. Photoacoustic techniques for trace gas sensing based on semiconductor laser sources[J]. Sensors, 2009, 9(12): 9616-9628.

[7] WILCKEN K, KAUPPINEN J. Optimization of a microphone for photoacoustic spectroscopy[J]. Applied Spectroscopy, 2003, 57(9): 1087-1092.

[8] MA Y F, QIAO S D, HE Y, et al. Highly sensitive acetylene detection based on multi-pass retro-reflection-cavity-enhanced photoacoustic spectroscopy and a fiber amplified diode laser[J]. Optics Express, 2019, 27(10): 14163-14172.

[9] KOSTEREV A A, BAKHIRKIN Y A, CURL R F, et al. Quartz-enhanced photoacoustic spectroscopy[J]. Optics Letters, 2002, 27(21): 1902-1904.

[10] WACLAWEK J P, MOSER H, LENDL B. Compact quantum cascade laser based quartz-enhanced photoacoustic spectroscopy sensor system for detection of carbon disulfide[J]. Optics Express, 2016, 24(6): 6559-6571.

[11] LANG Z T, QIAO S D, MA Y F. Acoustic microresonator based in-plane quartz-enhanced photoacoustic spectroscopy sensor with a line interaction mode[J]. Optics Letters, 2022, 47(6): 1295-1298.

[12] LIU K, GUO X Y, YI H M, et al. Off-beam quartz-enhanced photoacoustic spectroscopy[J]. Optics Letters, 2009, 34(10): 1594-1596.

[13] BÖTTGER S, KÖHRING M, WILLER U, et al. Off-beam quartz-enhanced photoacoustic spectroscopy with LEDs[J]. Applied Physics B, 2013, 113(2): 227-232.

[14] HU L, ZHENG C T, ZHENG J, et al. Quartz tuning fork embedded off-beam quartz-enhanced photoacoustic spectroscopy[J]. Optics Letters, 2019, 44(10): 2562-2565.

[15] MA Y F, HONG Y H, QIAO S D, et al. H-shaped acoustic micro-resonator based quartz-enhanced photoacoustic spectroscopy[J]. Optics Letters, 2022, 47(3): 601-604.

[16] MA Y F, HE Y, YU X, et al. HCl ppb-level detection based on QEPAS sensor using a low resonance frequency quartz tuning fork[J]. Sensors and Actuators B: Chemical, 2016, 233: 388-393.

[17] WU H P, SAMPAOLO A, DONG L, et al. Quartz enhanced photoacoustic H_2S gas sensor based on a fiber-amplifier source and a custom tuning fork with large prong spacing[J]. Applied Physics Letters, 2015, 107(11): 111104.

[18] MA Y F, HE Y, TONG Y, et al. Quartz-tuning-fork enhanced photothermal spectroscopy for ultra-high sensitive trace gas detection[J]. Optics Express, 2018, 26(24): 32103-32110.

[19] HU Y Q, QIAO S D, HE Y, et al. Quartz-enhanced photoacoustic-photothermal spectroscopy for trace gas sensing[J]. Optics Express, 2021, 29(4): 5121-5127.

[20] QIAO S D, HE Y, MA Y F. Trace gas sensing based on single-quartz-enhanced photoacoustic-photothermal dual spectroscopy[J]. Optics Letters, 2021, 46(10): 2449-2452.

[21] LIU K, MEI J X, ZHANG W J, et al. Multi-resonator photoacoustic spectroscopy[J]. Sensors and Actuators B: Chemical, 2017, 251: 632-636.

[22] LANG Z T, QIAO S D, HE Y, et al. Quartz tuning fork-based demodulation of an acoustic signal induced by photo-

thermo-elastic energy conversion[J]. Photoacoustics, 2021, 22: 100272.
[23] MA Y F, HE Y, ZHANG L G, et al. Ultra-high sensitive acetylene detection using quartz-enhanced photoacoustic spectroscopy with a fiber amplified diode laser and a 30.72 kHz quartz tuning fork[J]. Applied Physics Letters, 2017, 110(3): 031107.
[24] HE Y, MA Y F, TONG Y, et al. Ultra-high sensitive light-induced thermoelastic spectroscopy sensor with a high Q-factor quartz tuning fork and a multipass cell[J]. Optics Letters, 2019, 44(8): 1904-1907.
[25] HONG Y H, QIAO S D, MA Y F. Improved IP-QEPAS sensor based on cylindrical cavity enhancement[J]. Infrared Physics and Technology, 2021, 115: 103730.
[26] GORDON I E, ROTHMAN L S, HILL C, et al. The HITRAN2016 molecular spectroscopic database[J]. Journal of Quantitative Spectroscopy and Radiative Transfer, 2017, 203: 3-69.

Cylindrical Cavity-based Quartz-enhanced Spectroscopy Sensing (Invited)

LIANG Tiantian, HONG Yinghao, MA Yufei
(*National Key Laboratory of Science and Technology on Tunable Laser, Harbin Institute of Technology, Harbin* 150001, *China*)

Abstract: Gas sensing technology can detect gas concentration with high sensitivity and has significant application demands in the fields such as atmospheric chemistry, hazardous gas monitoring, etc. Compared with the non-spectral gas sensing technology, spectral technology utilizes the characteristic fingerprint spectrum of gas molecules, so it has excellent selectivity. The traditional photoacoustic spectroscopy technology employs the microphone as the acoustic detection element. However, the problems of the microphone itself, such as low Q value, wide response band, large background noise, and the large volume of the photoacoustic cell, restrict the practical application of this technology. In contrast to this, Quartz-Enhanced Photoacoustic Spectroscopy (QEPAS) and Light-Induced Thermoelastic Spectroscopy (LITES) take the Quartz Tuning Fork (QTF) as the acoustic wave detection element and light energy detection element respectively. Due to QTF having the characteristics of a narrow response frequency band (~4 Hz), high Q value (~10 000), an unnecessary photoacoustic cell, and so on, QEPAS has the advantages of anti-noise, small size, compact structure, low price, and so on, while LITES also has the advantage of non-contact detection. QEPAS and LITES have developed rapidly in recent years, and it has become a hotspot in gas sensing. Considering that both QEPAS and LITES technology can generate photoacoustic signals in the experiment and microresonators are usually devoted to increasing the acoustic signal strength. Therefore, in this manuscript, based on the resonance enhancement effect between the incident acoustic wave and the reflected acoustic wave, a non-one-dimensional resonant cylindrical cavity was designed to enhance the signal strength of the sensing systems and is first applied in out-of-plane incident QEPAS and LITES techniques. Firstly, the simulation model of QTF was established using the QTF size with the standard frequency of 32.768 kHz and was defined as a piezoelectric material. A cylindrical cavity was constructed near the QTF. Subsequently, the finite element analysis method was used in this paper. With and without adding the cylindrical cavity, respectively, to theoretically simulate and optimize the swing amplitude of the QTF and the position of the cylindrical cavity. The simulation results show that the QTF amplitudes in QEPAS and LITES are increased by 3.7 times and 1.9 times, respectively, after the addition of cylindrical cavities, compared with bare QTF. The experimental research, used a QTF with a standard resonant frequency of 32.768 kHz. Water vapour was selected as the target gas to test system performance, and its spectral line at 7 168.43 cm^{-1} with a line intensity of 1.196×10^{-20} cm/molecule was chosen as the target line to avoid interference from other gases in the air. A diode laser with an emission wavelength of 1.395 μm was adopted as the excitation source to match the water vapour absorption line. At this time, the output power of the laser was 18.9 mW. The low-frequency sawtooth wave output by a signal generator was employed for the coverage of the water vapour absorption line. The high-frequency sine wave generated by a lock-in amplifier was used to modulate the output wavelength. The two signals were superimposed and fed to the laser driver. The

lock-in amplifier also demodulated the piezoelectric signal generated by QTF into the second harmonic signal, and its integration time and rolling coefficient were set as 100 ms and 18 dB/oct, respectively. To obtain the best response from the system, all experimental results were measured at the resonance frequency of the QTF and the optimum modulation depth (0.43 cm^{-1}). To make full use of the acoustic waves generated by the photoacoustic effect, the cylindrical cavity was made of 304 stainless steel material with high reflectivity, and a small hole slightly larger than the size of the QTF was machined on the side of the cylindrical cavity so that the QTF can be put into the cavity. The Minimum Detection Limits (MDL) of QEPAS and LITES systems with the cylindrical cavity were 17.27 ppm and 7.21 ppm respectively. Compared to the bare QTF system without the cylindrical cavity, the performance is improved by 2.32 times and 1.27 times. The experimental result is slightly different from the theoretical simulation result, caused by the deviation of the mesh division degree in the simulation, the piezoelectric conversion efficiency and the resonance frequency of the QTF from the actual.

Key words: Quartz-enhanced photoacoustic spectroscopy; Light-induced thermoelastic spectroscopy; Cylindrical cavity; Gas Sensing; Quartz tuning fork

OCIS Codes: 300.6360; 300.6380; 300.6260; 140.2020

Foundation item: National Natural Science Foundation of China (Nos. 62022032, 61875047, 61505041), the Natural Science Foundation of Heilongjiang Province of China (No. YQ2019F006), the Postdoctoral Fund of Heilongjiang Province (No. LBH-Q18052), the Fundamental Research Funds for the Central Universities